ARTICLE

Glass engineering of aminotriazine-based materials with sub-ambient T_g and high kinetic stability

Received 00th January 20xx,
Accepted 00th January 20xx

DOI: 10.1039/x0xx00000x

Zeinab Kara Ali,[a] Anna Iankovitch,[b] Mahboubeh Jokar,[b] Thierry Maris,[a] Olivier Lebel,*[b] Christian Pellerin*[a]

A challenge in glass engineering is the design of molecular glasses combining a high glass kinetic stability (GS) of the amorphous phase with a low (sub-ambient) glass transition temperature (T_g). Triazine derivatives with arylamino substituents readily form glassy phases that can show outstanding resistance to crystallization. In the present study, a series of 12 analogous compounds incorporating phenylamino and cyclohexylamino groups was synthesized, and their thermal properties and intermolecular interactions were studied. All compounds possess an excellent glass-forming ability, a low T_g ranging from 32 °C to as low as -19 °C, and a high GS. While the cyclohexyl derivatives show higher T_g, the phenyl derivatives possess a higher GS with some compounds remaining completely amorphous for over three years despite their sub-ambient T_g. X-ray diffraction, infrared spectroscopy and DFT calculations reveal that the higher volume occupancy and rotational energy barrier of cyclohexyl groups are the main factors responsible for the compounds' higher T_g values but that they also contribute to their higher propensity to crystallize. In counterpart, the planarity of phenyl groups leads to poorer packing and enhances their GS while keeping their T_g well below ambient. The formation of hydrogen bonds or competing interactions provides an additional handle to tune the T_g of the compounds. Taken together, these studies provide guidelines for the design of molecular glasses with readily tunable thermal properties in view of their functionalization.

Introduction

The glassy state is ubiquitous in materials science but many questions remain unanswered despite a recent reinvigorated interest. [1, 2] This is partly due to the out-of-equilibrium amorphous nature of glasses, which originate from a poorly ordered arrangement at the molecular level.[3-5] Glass formation occurs when the sample can reach an arrested solid-like state, either by cooling from the melt or by evaporation from solution, before crystal nucleation and growth can occur.[1, 6-8] The solid is then kinetically trapped in a distribution of molecular arrangements reminiscent of a liquid, but without the molecular mobility required for the molecules to rapidly converge towards a thermodynamically stable (crystalline) state. This crystallization process is only decelerated and eventually occurs in a time scale that can range from a few hours to arguably millions of years in extreme cases.[2]

Several polymers and inorganic solids possess the ability to readily form glasses due to their chain entanglements and to their extended tridimensional network structures, respectively, that hinder crystallization.[9] Glass formation in small organic molecules remains more elusive as they tend to readily crystallize due to their higher molecular mobility, highlighting the subtle interplay between kinetic and thermodynamic factors at work in the formation and long-term subsistence of the glassy state.[3-5, 10]

Small organic molecules that can readily form glassy phases and that remain amorphous for extended periods of time are called molecular glasses, or amorphous molecular materials.[11-13] They are used for several applications ranging from pharmaceutical formulations[14, 15] to nanolithography[16], photonics, and organic electronics[11, 17]. Indeed, the monodisperse nature of small molecules, compared to polymers, leads to easier purification, characterization, and processing, as well as to higher batch homogeneity. For these practical applications, it is crucial to ensure that the amorphous state is maintained well beyond the expected lifetime of the device or formulation because crystallization could dramatically affect the properties and performance of the system. For this reason, insights on how the molecular structure impacts the bulk properties of molecular glasses (including their glass transition temperature, T_g),[18-20] and how it can lead to undesirable crystallization, are extremely valuable.[21-23] Some structural guidelines have emerged to design compounds with a higher propensity toward glass formation: irregular and globular structures, low molecular symmetry, and the presence of multiple conformations.[10, 12, 19, 22] While these guidelines are fairly accurate, designing new molecular glasses still relies on a trial and error component, and structures identified as promising candidates for glass formation can still crystallize in counterintuitive ways.

[a] Département de chimie, Université de Montréal, Montréal, QC, H3C 3J7, Canada. Email: c.pellerin@umontreal.ca
[b] Department of Chemistry and Chemical Engineering, Royal Military College of Canada, Kingston, ON, K7K 7B4, Canada. Email: olivier.lebel@rmc.ca

Electronic Supplementary Information (ESI) available: Additional crystallographic information and crystal structure views, DFT calculation results, and infrared spectroscopy and NMR data. See DOI: 10.1039/x0xx00000x

Our group has developed a class of molecular glasses based on aminotriazines that shows outstanding glass-forming ability (GFA) and high resistance to crystallization.[24, 25] These compounds are relatively small and can tolerate an unusually high degree of symmetry as well as the presence of extensive hydrogen bonding. A representative structure is shown in Scheme 1 where the triazine possesses one small "headgroup" (HG) at the 2-position, which can be a variety of functional groups with a short alkyl chain, and two larger amino substituents on the 4- and 6- positions, termed "ancillary groups" or "tail groups". Typically, one of these groups (R1) must be an arylamino group, while the other (R3) can be an alkylamino or arylamino group.[26, 27] The amino group linkers can be N-methylated (R2 = CH_3) without loss of glass-forming ability, but with substantially lower T_g values because of the lack of hydrogen bonds in the solid state.[28] The main structural element contributing to their excellent GFA was identified to be the presence of multiple conformers of similar energy coupled with a high interconversion barrier resulting from strong conjugation of the amino groups to the triazine ring.[28] This leads to statistical populations of different conformers in the solid or supercooled liquid state which make it very difficult to converge to the ordered arrangement required to nucleate a crystal. The presence of hydrogen bonds in some derivatives exacerbate this by generating small aggregates that do not pack efficiently and in which conformational interconversion is further hindered.[29, 30]

Scheme 1. Structural framework of triazine-based molecular glasses.

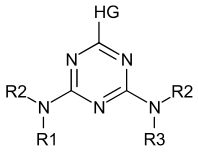

Some structural elements are not as efficient at promoting glass formation. For example, headgroups that are either too small or too large result either in compounds that require very fast cooling to form glasses (and thus present a poor GFA), or that form glasses that readily recrystallize when held above T_g.[25] For compounds with secondary amino ancillary groups, the 3,5-dimethylphenyl (mexyl) group was identified as the best for glass formation. Most compounds whose aryl groups do not contain at least one *meta* substituent were found to crystallize above T_g, or even within a few days on standing below T_g in some cases.[27] Worse still, compounds with two alkylamino ancillary substituents, such as cyclohexylamino groups, are more likely to crystallize than their aryl analogues.[27] The reasons behind this behavior are not yet understood so probing the structural differences between closer analogues can yield important insight on the impact of selected structural elements on glass formation as opposed to crystallization.

Herein, we probe the impact of alkyl vs. aryl substitution by synthesizing and characterizing a library of 12 analogues containing phenyl or cyclohexyl ancillary substituents and 4 different headgroups. All compounds show an excellent glass-forming ability (GFA) but different glass kinetic stability (GS). In particular, replacing phenyl ancillary substituents by cyclohexyl groups has two marked effects on the properties of the amorphous materials: 1) it increases T_g due to the higher interconversion barrier of cyclohexyl groups, and 2) it favors crystallization due to their increased volume, thereby leading to more efficient packing in the solid state. The crystal structures of selected cyclohexyl-containing derivatives were determined and show close-packed structures with few directional interactions between molecules. The addition of hydrogen bond-donating headgroup can finally be used to tune T_g below or above ambient and to further reduce the propensity to crystallize.

Results and discussion

Synthesis

A library of 12 analogous triazine derivatives was designed to study the impact of the ancillary groups (alkyl or aryl) on their glass-forming ability. Triazine derivatives with an NH linker and with phenyl and cyclohexyl ancillary groups have previously been synthesized and studied [27] but they were found to show similar T_g values and to crystallize relatively quickly. Here, N-methylated symmetric analogues were synthesized using N-methylphenylamino (**1_{HG}**) and N-methylcyclohexylamino substituents (**3_{HG}**), while an asymmetrically substituted series was prepared with one N-methylphenylamino group and one N-methylcyclohexylamino group (**2_{HG}**) (Scheme 2). As previous studies have shown that the rotational energy barrier of the headgroup (HG) has a pronounced impact on T_g,[31] four series of compounds were synthesized with the following headgroups: Et, OMe, NMe_2, and NHMe. Only compounds with the NHMe headgroup can form hydrogen bonds, thereby allowing to probe the formation and impact of hydrogen bonds with greater detail than when multiple NH groups are present.

Scheme 2. Structures of the new compounds used in the present study.

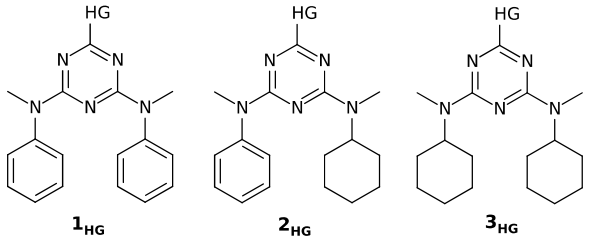

Symmetrically substituted compounds **1_{HG}** and **3_{HG}** were synthesized by a series of sequential nucleophilic substitutions on cyanuric chloride. The headgroups were first introduced following literature procedures using either methylamine or dimethylamine in acetone, sodium methoxide in methanol, or ethylmagnesium chloride in dry ether, to yield the corresponding monosubstituted 4,6-dichloro-1,3,5-triazines (Scheme 3).[26, 32-34] The amino ancillary groups were then

introduced using an excess of either N-methylaniline (1_{HG}) or N-methylcyclohexylamine (**3_{HG}**) in refluxing THF (Scheme 3).

Scheme 3. Synthesis of compounds **1_{HG}** and **3_{HG}**.

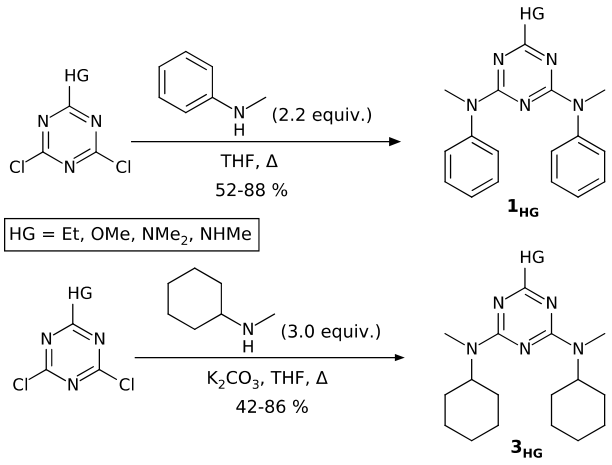

For unsymmetrically substituted compounds **2_{HG}**, disubstituted precursor **4** was first synthesized by reacting N-methylphenylamino-4,6-dichloro-1,3,5-triazine[35] with N-methylcyclohexylamine in acetone at ambient temperature. Precursor **4** was then reacted with either excess methylamine or dimethylamine in refluxing THF to afford compounds **2_{NHMe}** and **2_{NMe2}**, or with sodium methoxide in refluxing methanol to yield compound **2_{OMe}** (Scheme 4). For ethyl-substituted derivative **2_{Et}**, 2-ethyl-4,6-dichloro-1,3,5-triazine (see above) was reacted with N-methylcyclohexylamine in acetone at ambient temperature to yield precursor **5**, followed by N-methylaniline in refluxing THF to yield compound **2_{Et}** (Scheme 5).

Scheme 4. Synthesis of compounds **2_{OMe}**, **2_{NHMe}** and **2_{NMe2}**.

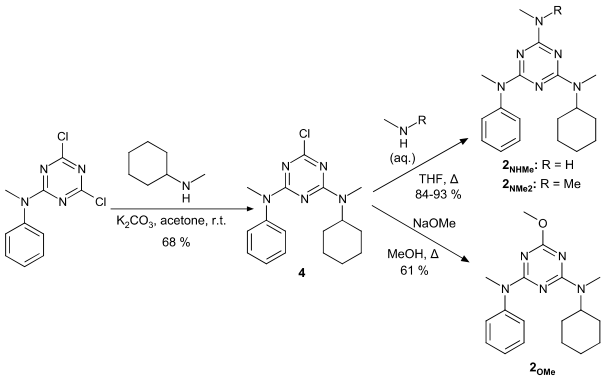

The synthetic procedures used allowed for an easy separation of the desired products from secondary products or unreacted reagents. Excess cyanuric chloride could be hydrolyzed by washing with aqueous NaOH, whereas unreacted amines could be removed by washing with aqueous HCl or acetic acid. Monochloro intermediates **4** and **5** could be readily recrystallized from hexanes.

Scheme 5. Synthesis of compound **2_{Et}**.

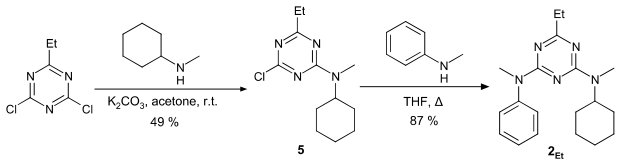

Thermal Properties

Differential scanning calorimetry (DSC) was used to study the glass-forming properties of compounds **1_{HG}**-**3_{HG}**. DSC was first used to determine the critical cooling rate (*Rc*) of the compounds, which is defined as the slowest cooling rate at which the compound does not crystallize, to determine their respective glass-forming ability (GFA). Good glass-formers do not crystallize even when cooled at very slow rates. The twelve compounds synthesized herein did not show any signs of crystallization when cooled at rates as slow as 0.5 °C/min, thereby showing their outstanding GFA. Furthermore, no crystallization was observed when heating any of the compounds at a rate of 10 °C/min. In contrast, previously reported analogues **6_{HG}** -**7_{HG}** (Scheme 6), with NH linkers instead of NMe linkers, all readily crystallized upon heating, and only derivative 6_{NHMe} presented an *Rc* value below 5 °C/min.[27] Derivative **7_{Et}** failed to form a glass even when quenched from the liquid state at a rate as fast as 100 °C/min. The presence of the NMe linkers in compounds **1_{HG}**-**3_{HG}**, and the concurring elimination of hydrogen bonds, results in a higher propensity to form glasses, even in the absence of additional substituents on the phenyl or cyclohexyl rings. This result highlights the complex role that hydrogen bonding plays in glass engineering. On one hand, the presence of multiple H-bonding sites can favor vitrification by forming highly irregular H-bonded aggregates, for instance in many sugars. On the other hand, it can also promote crystallization by ordering the molecules in a crystalline-like aggregated structure in the absence of competing H-bonding patterns or other structural elements that frustrate regular packing.

Scheme 6. Structures of compounds **6**-**7**.

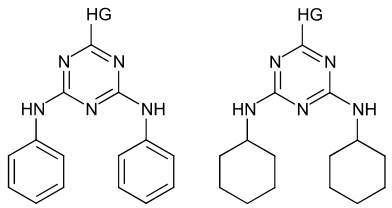

DSC was then used to measure the glass transition temperatures (Figure 1) and melting temperatures (Table 1) of compounds **1_{HG}**-**3_{HG}**. The T_g values range from -19 to 32 °C and

are all much lower (by between 26 to 49 °C) than those of their analogues with NH linkers, emphasizing the large impact of hydrogen bonding on the T_g of molecular glasses. Consistently, the compounds with the NHMe headgroup show a T_g significantly higher (by 15 – 28 °C) than their analogues, which is due to the formation of hydrogen bonds as demonstrated below by IR spectroscopy. H-bonds are completely absent for compounds with the other headgroups. The effect of the headgroup on T_g also mirrors the trends previously observed for compounds with NH linkers, where headgroups more strongly conjugated to the triazine core result in higher T_g because of their higher activation energy for rotation.[28, 31] The exception to this trend is the NMe_2 headgroup, which shows lower T_g values than the OMe headgroup even though its DFT calculated rotational energy barrier is higher (-63 kJ/mol vs 33 kJ/mol). This may be a result of the steric hindrance generated by the additional Me substituent in the bulk state, an effect that is not captured by our calculations in vacuo.

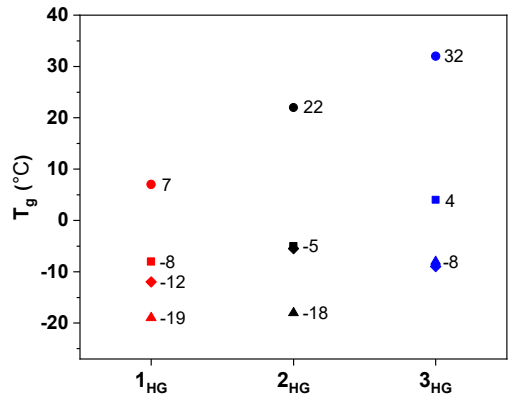

Figure 1. Glass transition (T_g) temperatures of compounds $\mathbf{1_{HG}}$ -$\mathbf{3_{HG}}$. (Circles: NHMe, squares: OMe, diamonds: NMe_2, triangles: Et).

The nature of the ancillary groups also affects the T_g values of compounds with the same headgroup. Interestingly, the cyclohexyl-substituted compounds $\mathbf{3_{HG}}$ all show higher T_g values than their analogues with two phenyl groups $\mathbf{1_{HG}}$. Mixed compounds $\mathbf{2_{HG}}$ show T_g values intermediate between their diphenyl ($\mathbf{1_{HG}}$) and dicyclohexyl ($\mathbf{3_{HG}}$) analogues. This effect is exacerbated with a NHMe headgroup, where there is a 25 °C difference between the T_g of the $\mathbf{1_{NHMe}}$ and $\mathbf{3_{NHMe}}$ derivatives. These observations mirror the trend observed in related polymers, where poly(vinylcyclohexane) shows a T_g value ~30 °C higher than that of closely related polystyrene with similar degrees of polymerization.[36] In this work, the authors have concluded that cyclohexyl groups led to higher T_g values because of their larger size and capacity to adopt multiple conformations, which would both help pack more efficiently. However, this trend contrasts the results obtained with analogous triazine derivatives $\mathbf{6_{NHMe}}$ and $\mathbf{7_{NHMe}}$ with NH linkers (scheme 6), where the diphenyl (56 °C) and dicyclohexyl (58 °C) derivatives showed almost identical T_g values.[27] In that case, it is likely that the dominant factor for influencing T_g is the presence of extended hydrogen bonding with the NH linkers, thereby strongly mitigating the influence of the phenyl or cyclohexyl substituents. In contrast, the NMe linkers used here allow to more fully express the effect of the ancillary groups. We have previously noted a similar effect when comparing compounds with stilbene and pentafluorostilbene ancillary groups.[37] The compounds had a large T_g difference of 17 °C in the presence of a headgroup unable to H-bond (NMe_2), but this T_g difference vanished when the NHMe headgroup participated in H-bonding.

Long-term glass kinetic stability (GS) was monitored by probing the presence of crystals in the samples after storing for three years at ambient temperature in DSC pans. Most molecular glasses tend to crystallize slowly at ambient temperature in the glassy state, but substantially faster when heated above their T_g because of the increased molecular mobility in the supercooled liquid state. For compounds with sub-ambient T_g, it is therefore crucial to possess a very high GS to remain amorphous at room temperature. The results in Table 1 reveal the diphenyl derivatives $\mathbf{1_{HG}}$ display outstanding GS in spite of their sub-ambient T_g as they remained completely amorphous. In fact, a melting temperature was never found for any of the $\mathbf{1_{HG}}$ samples processed under various conditions. In contrast, two of the dicyclohexyl derivatives $\mathbf{3_{HG}}$ were semi-crystalline after long-term storage while the other two remained amorphous. The mixed derivatives $\mathbf{2_{OMe}}$, $\mathbf{2_{Et}}$ and $\mathbf{2_{NHMe}}$ also remained completely amorphous while $\mathbf{2_{NMe2}}$ crystallized. These observations clear demonstrate that aryl ancillary groups provide better kinetically stable glasses than their alkyl counterparts despite their lower T_g. Interestingly, while previous observations show that lowering the degree of molecular symmetry tends to improve glass kinetic stability, we find in the present case that the impact of alkyl ancillary groups on promoting crystallization supersedes the impact of lowering molecular symmetry.

Table 1. Long-term glass stability of compounds $\mathbf{1_{HG}}$ - $\mathbf{3_{HG}}$ after aging for three years at ambient temperature (A: amorphous, S: semi-crystalline and C: crystalline).

Headgroup	1		2		3	
	State	T_m (°C)	State	T_m (°C)	State	T_m (°C)
Et	A	---	A	---	A*	65
OMe	A	---	A	---	S	67
NMe_2	A	---	C	97	S	54
NHMe	A	---	A*	79	A*	94

Crystal Structures

Even though compounds $\mathbf{1_{HG}}$-$\mathbf{3_{HG}}$ all readily form glasses and do not crystallize when annealed above T_g for short (or highly extended) periods of time, crystals suitable for X-ray diffraction could be grown by slow evaporation from methanol for compounds $\mathbf{3_{Et}}$, $\mathbf{3_{OMe}}$ and $\mathbf{3_{NMe2}}$, or from chloroform for compound $\mathbf{2_{NMe2}}$.[38]

Table 2. Crystallographic parameters for single crystals compounds $\mathbf{3_{Et}}$, $\mathbf{3_{OMe}}$, $\mathbf{3_{NMe2}}$ and $\mathbf{2_{NMe2}}$, crystallized by slow evaporation from methanol or from chloroform.

Compound	$\mathbf{3_{Et}}$	$\mathbf{3_{OMe}}$	2_{NMe2}	3_{NMe2}
Space Group	*Pbca*	*Pbca*	$Pca2_1$	$P2_1/m$
a (Å)	15.0700(3)	14.7113(3)	14.6085(5)	5.7373(3)
b (Å)	10.3551(2)	10.5414(2)	12.2750(4)	30.1441(16)
c (Å)	24.4042(5)	24.3585(6)	10.4746(4)	6.1322(3)
β (°)	90	90	90	109.223(3)
Volume (Å^3)	3808.31(13)	3777.46(14)	1878.30(11)	1001.41(9)
Z	8	8	4	2
Density (g.cm^{-3})	1.156	1.173	1.204	1.149
Packing Index (%)	67.6	66.5	67.4	66.2

Compounds $\mathbf{3_{Et}}$ and $\mathbf{3_{OMe}}$ both crystallized in the orthorhombic space group *Pbca*, both with 8 molecules per unit cell and very close unit cell dimensions (Table 2; more detailed information can be found in Table S1). In both cases, the molecules (individual molecules are shown in Figure 2 and the their respective thermal atomic displacement ellipsoid plots are shown in Figures S1-S4) crystallized in a close-packed lamellar structure composed of bidimensional sheets where molecules are oriented in a corrugated array of unidimensional stacks arranged in an alternating head-to-tail fashion, presumably to maximize space filling (Figure S5). Unsymmetrical analogue $\mathbf{2_{NMe2}}$ crystallized in the orthorhombic space group $Pca2_1$, with 4 molecules per unit cell. Again, the crystal packing is strikingly similar to that of compounds $\mathbf{3_{Et}}$ and $\mathbf{3_{OMe}}$, with the molecules arranged in the same type of lamellar structure (Figure S5). On the other hand, dimethylamino derivative $\mathbf{3_{NMe2}}$ crystallized in the monoclinic space group $P2_1/m$, with two molecules per unit cell. Again, the molecules form lamellar structures consisting of intercalated sheets (Figure S5). Notably, compound $\mathbf{3_{NMe2}}$ crystallized with the molecules in a different conformation: both ancillary group rings point in the same direction as the headgroup (top-top conformation), rather than in the opposite direction (bottom-bottom conformation) as for the three other compounds (Figure 2). The adoption of this top-top conformation by $\mathbf{3_{NMe2}}$ is likely a result from the steric hindrance caused by the additional methyl substituent from the headgroup (which may be compensated by the smaller phenyl group in compound $\mathbf{2_{NMe2}}$). This steric hindrance may also prevent efficient packing in other conformations and explain the anomalous trend of T_g observed for the NMe_2 headgroup where mixed derivative $\mathbf{2_{NMe2}}$ shows a higher T_g than its bis(cyclohexyl) analogue $\mathbf{3_{NMe2}}$.

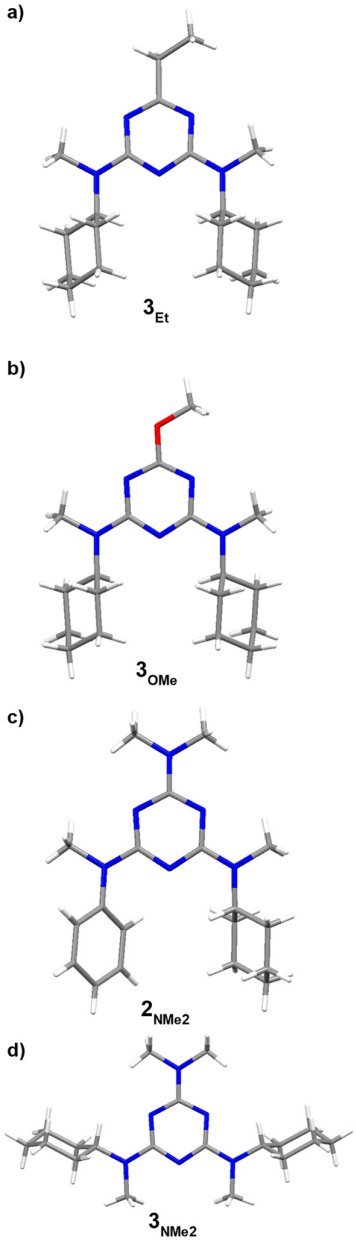

Figure 2. View of individual molecules from the crystal structures of compound a) $\mathbf{3_{Et}}$, b) $\mathbf{3_{OMe}}$, c) $\mathbf{2_{NMe2}}$, and d) $\mathbf{3_{NMe2}}$. The molecules are in the bottom-bottom conformation for a)-c), and in the top-top conformation for d).

Interestingly, no notable interactions to direct the molecular packing in a specific fashion seem to exist in the crystal structures of compounds $\mathbf{3_{Et}}$, $\mathbf{3_{OMe}}$, $\mathbf{3_{NMe2}}$ and $\mathbf{2_{NMe2}}$. The packing is instead likely a result of the optimal utilization of space. Even in the structure of compound $\mathbf{2_{NMe2}}$, which contains an electron-rich phenylamino group and an electron-deficient triazine ring, no π–π stacking can be observed, neither face-to-face interactions between the phenyl and triazine rings, nor edge-to-face interactions between the phenyl rings. Presumably, as these interactions are relatively weak, filling all the available space proves more advantageous enthalpically for the system.

The Kitaigorodskii packing indices[39] of the four crystal structures were calculated using the CALC SOLV routine of the Platon software suite[40, 41] and are listed in Table 2. For all four compounds, the values range from 66.2 to 67.6 %, which are all above the "usual" value of 65 % for organic crystals. These values, coupled with the fact that the compounds crystallize in close-packed structures with no included solvent molecules, highlight the previous observations that in these cases, crystallization is driven by optimizing packing rather than by the formation of specific intermolecular interactions. Interestingly, the only compound in the dicyclohexyl series that can participate in hydrogen bonding, **3_{NHMe}**, is the only compound for which high-quality single crystals could not be successfully grown, highlighting the complex role of hydrogen bonding in both promoting and hindering the crystallization process.

The Hirshfeld surfaces, which represent the space proper to each molecule as well as a map for intermolecular interactions, were also calculated for the four crystal structures and are shown in Figure 3.[42-45] They confirm the absence of major intermolecular interactions, the closest contacts observed in all cases being interactions between NMe groups and triazine C atoms. However, such close contacts seem to stem from the packing of the molecules itself rather than from a driving force that directs molecular assembly. The fact that only one or two of the NMe groups are in close proximity to the triazine ring tends to confirm this. The fingerprint plots, which represent the intermolecular distances for contacts between atoms from neighboring molecules, are presented in terms of di (distance between the Hirshfeld surface and the internal atom) vs. de (distance between the Hirshfeld surface and the external atom) (Figure 4). In all cases there is a narrow distribution of contact distances, with no clear short or long contacts that may hint towards the presence of strong and directional interactions, or conversely to the presence of empty pockets in the structures.

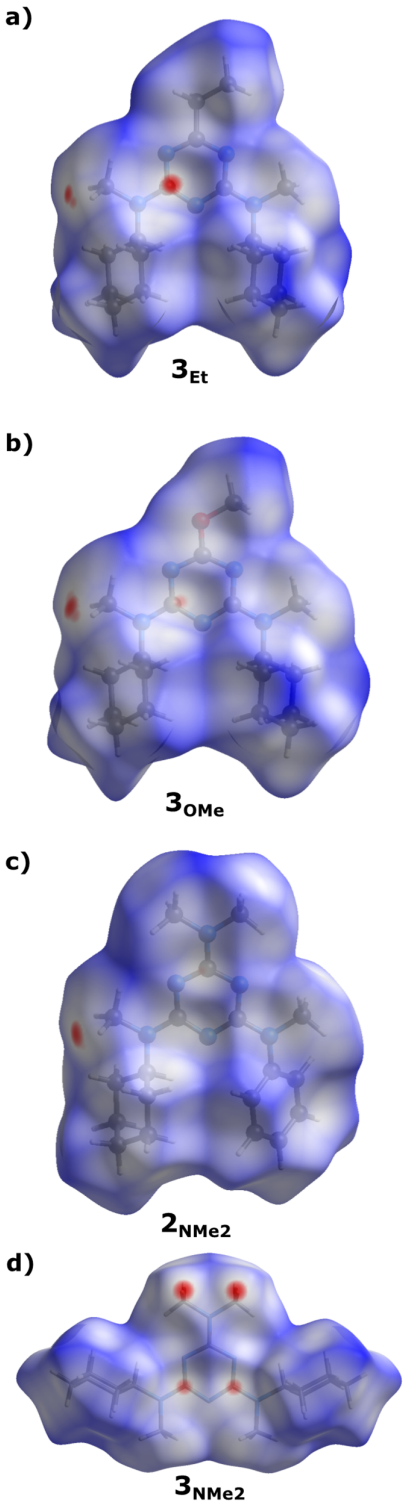

Figure 3. Hirshfeld surfaces mapped with normalized contact distance (d_{norm}) for single molecules in the crystal structures of compounds a) 3_{Et}, b) 3_{OMe}, c) 2_{NMe2}, and d) 3_{NMe2}.

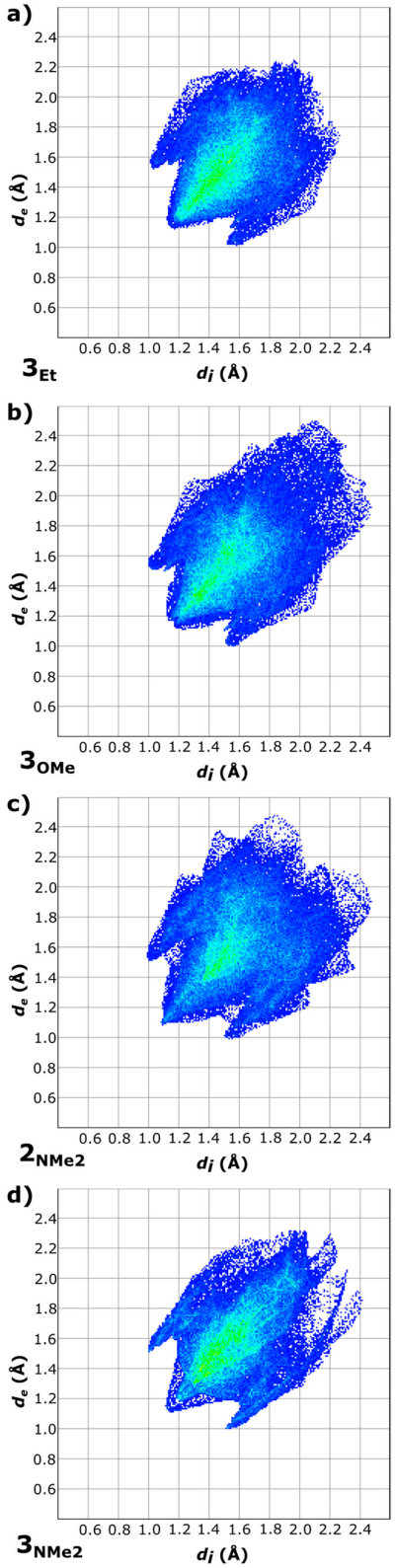

Figure 4. Fingerprint plots for the crystal structures of compounds a) $\mathbf{3}_{Et}$, b) $\mathbf{3}_{OMe}$, c) $\mathbf{2}_{NMe2}$, and d) $\mathbf{3}_{NMe2}$.

Calculation of Rotational Energy Barriers

The principal structural factor contributing to glass formation in aminotriazine derivatives has been identified to be the formation of multiple conformers of similar energy with high interconversion barriers.[28, 30, 31] The rotational barrier of the headgroup was also found to strongly correlate with T_g.[31] It is therefore plausible that the rotational barrier of the ancillary groups has a similar impact on T_g. The rotational barriers were calculated using DFT [B3LYP with a 6-31g(d,p) basis set; similar results were obtained in select cases using a 6-311+g(d,p) basis set], by calculating the energy of the molecules while varying the dihedral angle of the linker relative to the triazine ring. Both arylamino and alkylamino groups show high rotational barriers due to strong conjugation with the triazine ring. Figure 5a shows a representative example of the calculated energies for compound $\mathbf{3}_{NMe2}$ along with illustrations in Figure 5b of its three stable conformers (bottom-bottom, top-bottom and top-top). Figure 5c shows that the compounds with phenylamino groups have a lower rotational barrier of 47-53 kJ/mol, depending on the headgroup, than compounds with cyclohexylamino groups (68-74 kJ/mol). These rotational energy barriers calculated by DFT on individual molecules fall within the range of values calculated by molecular dynamics simulations[26] on cells of 40 molecules of analogous compounds (where the linkers were NH groups and not NMe groups as in this work). The values are also close to values measured experimentally on simple aminotriazines by variable-temperature NMR.[46] The higher activation energy for the cyclohexyl-substituted compounds implies less interconversion events between conformers and therefore contributes to increasing their T_g compared to the analog compounds with phenyl ancillary groups. Interestingly, this rotational barrier is lower with the amino headgroups (NHMe or NMe_2) than with the ethyl or methoxy headgroups, likely a consequence of the headgroups' own resonance with the triazine ring.

Previous studies have suggested that in addition to high interconversion barriers, the presence of multiple conformers with similar energy is crucial to both a high GFA and a high GS in triazine-based molecular glasses. Our calculations indeed reveal very close energy (within 3 kJ/mol, see Table S2) for the three stable conformers (top-top, top-bottom and bottom-bottom) of any given compound (illustrated in Figure 5a-b for two conformers of compound $\mathbf{3}_{NMe2}$). This explains the excellent glass-forming ability of all the studied compounds and their good to outstanding glass kinetic stability. It also puts in perspective the fact that compound $\mathbf{3}_{NMe2}$ crystallized with a different conformation than the other compounds for which a crystal structure could be determined. In fact, this suggest that polymorphism may be possible in this class of compounds, although it was not observed experimentally as their excellent GFA makes their crystallization very difficult to study. Compounds with cyclohexyl groups show an even higher interconversion barrier than those with phenyl groups, yet show lower GS, which seems at first glance contradictory with our previous results.[28] Ultimately, these observations can be rationalized by the fact that crystallization will be facilitated by

the presence of more efficiently packing motifs, even if that process is retarded by slow conformational equilibria. As shown in Figures 4 and S5, the dicyclohexyl derivatives show compact crystal structures, even in the absence of directing intermolecular interactions; in this case, the high interconversion barriers are likely to frustrate crystallization to a certain extent, but the molecules will eventually converge towards an ordered structure.[8]

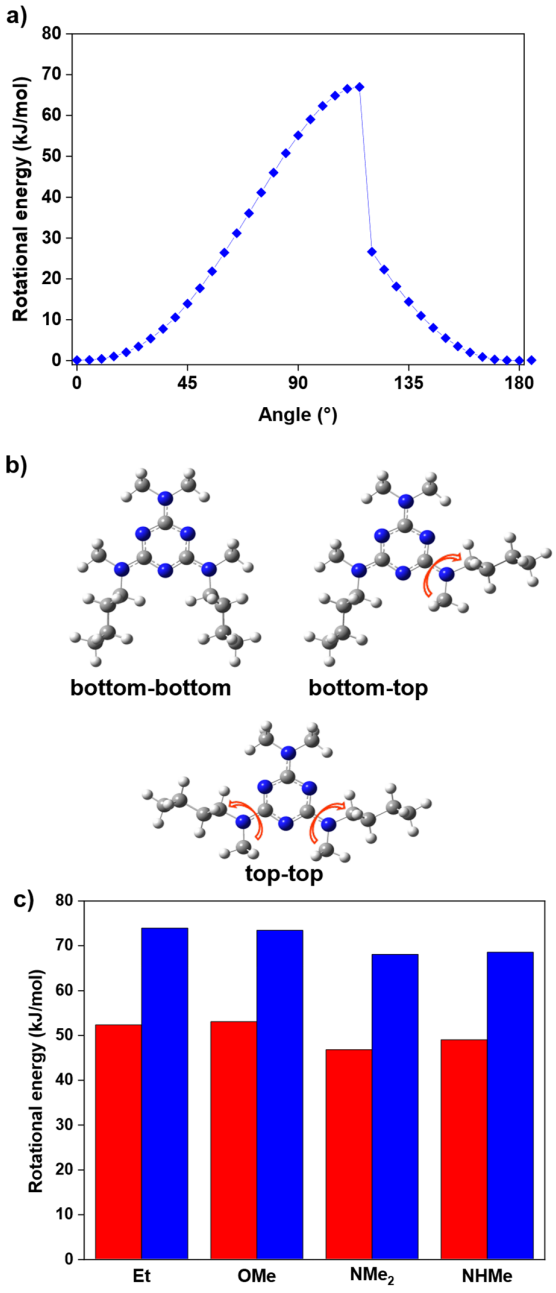

Figure 5. a) Example of a dihedral angle sweep for compound $\mathbf{3}_{NMe2}$ in the bottom-bottom conformation determined by DFT calculations, b) illustration of its three most stable conformations and c) rotational energy barriers for the N-methylphenyl (red) and N-methylcyclohexyl (blue) groups for compounds $\mathbf{1}_{HG}$ and $\mathbf{3}_{HG}$.

Impact of Hydrogen Bonding

We have previously used variable-temperature infrared (IR) spectroscopy, coupled with chemometrics analysis, to monitor the formation of hydrogen bonds while aminotriazine-based molecular glasses undergo their glass transition.[28] The fraction of NH groups forming hydrogen bonds was shown to increase steadily upon cooling from the viscous state, at the expense of the "free" NH groups (not engaged in H-bonds), and to reach up to 70-85 % at T_g. A slower increase in the fraction of H-bonded NH groups was observed upon further cooling below T_g. We also found a direct correlation between the value of T_g and the average number of H-bonded NH groups per molecule.

In the current series of compounds, only NHMe-substituted derivatives $\mathbf{1}_{NHMe}$-$\mathbf{3}_{NHMe}$ contain an NH group susceptible of forming such hydrogen bonds. These three compounds show much higher T_g than their analogues with other headgroups. Their H-bonding behavior was therefore investigated by IR spectroscopy upon cooling from 33 °C above T_g down to 32 °C below T_g at a rate of 2 °C/min. Figure 6 shows that compounds $\mathbf{1}_{NHMe}$-$\mathbf{3}_{NHMe}$ all feature an H-bonded N-H band centered around 3282 cm^{-1} whose relative intensity increases upon cooling from the viscous state to the glassy state. However, the "free" N-H band present at higher wavenumbers show clear differences in shape and position between the compounds. The "free" N-H band of diphenyl-substituted $\mathbf{1}_{NHMe}$ is located at 3432 cm^{-1} and is very similar to that of the previously reported compound also bearing a NHMe headgroup and aromatic ancillary mexyl groups (but with NH linkers as opposed to NMe linkers for $\mathbf{1}_{NHMe}$).[28] On the other hand, in the case of dicyclohexyl derivative $\mathbf{3}_{NHMe}$, the "free" N-H band is notably blue-shifted by 30 cm^{-1}, indicating that its NH groups are less affected by intermolecular interactions. Finally, the compound $\mathbf{2}_{NHMe}$ bearing a phenyl ring and a cyclohexyl ring shows both "free" bands (Figure 6). The "free" N-H band is therefore composed of a combination of two components at around 3462 cm^{-1} due to weakly interacting groups and at 3432 cm^{-1} for NH groups presumably engaged in NH – π interactions with phenyl groups.[47, 48] To validate this attribution, the IR spectrum of compound $\mathbf{3}_{NHMe}$ was recorded in 1 mM chloroform and toluene solutions (Figure S6). The absence of a band around 3282 cm^{-1} confirms that the concentration is low enough to prevent the molecules from engaging in hydrogen bonding. The spectrum of the sample in chloroform shows a single N-H band at 3460 cm^{-1} while the sample in toluene shows both "free" bands at 3457 and 3440 cm^{-1}, confirming their attribution to NH groups forming only weak van der Waals interactions and engaged in stronger NH – π interactions, respectively. The results thus confirm the presence of NH – π interactions in the glassy state and in the viscous state for the compounds containing aromatic ancillary groups.[48, 49] This observation helps explain the previously reported trend in which compounds with NH linker groups were better glass-formers in the presence of aromatic ancillary groups than with alkyl ancillary groups because they provide additional non-directing interactions.[27] However, these interactions are not necessary for the formation of kinetically

stable glasses, as many analogous compounds without NH groups also show a very high glass stability.

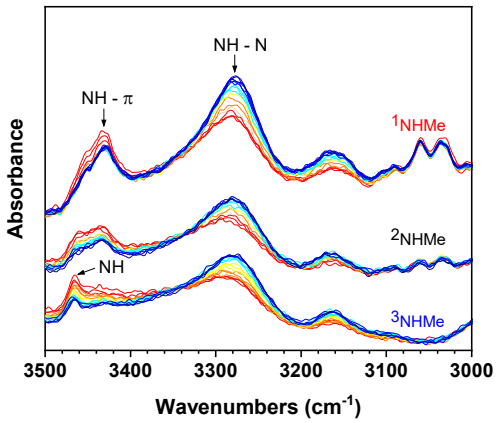

Figure 6. Variable-temperature IR spectra of compounds $\mathbf{1}_{NHMe}$-$\mathbf{3}_{NHMe}$ at temperatures ranging from T_g + 33 °C (red traces) to T_g - 32 °C (blue traces). The bands due to NH groups engaged in hydrogen bonding (NH – N), NH – π interactions, and weak van der Waals interactions (NH) are indicated.

Figure 7a shows that upon cooling $\mathbf{2}_{NHMe}$ from the viscous state toward the glassy state, the fraction of H-bonded NH groups increases gradually from less than 50 % to close to 70 %. The formation of H-bonds occurs at the expense of both the free NH and NH – π interacting groups. A change of slope is apparent upon reaching T_g at 22 °C. Below this temperature, the rate of H-bond formation decreases due to the much higher viscosity in the glassy state that hinders further molecular rearrangements and prevents from forming an ideal glass. Similar plots for compounds $\mathbf{1}_{NHMe}$ and $\mathbf{3}_{NHMe}$ are shown in Figure S7. Figure 7b shows that analogous trends are present for the H-bonded NH groups of compounds $\mathbf{1}_{NMHe}$ and $\mathbf{3}_{NHMe}$. A notable feature of Figure 7b is that the fraction of H-bonded NH groups is essentially the same (within 1.3 %) for the three compounds when heated well into the viscous state at T_g + 33 °C but that substantial differences exist in the glassy state. At 32 °C below T_g, the H-bonded fraction is 16 % larger for $\mathbf{3}_{NHMe}$ with two cyclohexyl rings than for $\mathbf{1}_{NHMe}$ with two phenyl rings (Table S3). While H-bonds predominate in the glassy state for all compounds, a significant portion of the NH groups form weaker NH – π interactions with nearby phenyl groups for compounds $\mathbf{2}_{NHMe}$ and especially $\mathbf{1}_{NHMe}$. In other words, the fraction of H-bonded NH groups that must be reached for the glass transition phenomenon to occur during cooling is decreased by the presence of competing interactions. This lower number of H-bonds per molecule contributes, in turn, to decreasing the T_g of the phenyl-containing compounds. This would explain why the compounds with the NHMe headgroup show a larger effect of the ancillary groups on T_g (Figure 1) than the derivatives with other headgroups that cannot form hydrogen bonds. This detrimental effect of NH – π interactions on T_g is mitigated in compounds with NH linkers, such as compounds $\mathbf{6}_{NHMe}$ and $\mathbf{7}_{NHMe}$,[27, 37] because the average number of hydrogen bonds per molecule is higher overall.

Attempts were also made to monitor changes in the C-H, C-C or C-N bands for compounds without NH groups but proved unfruitful as slight shifts in these signals could not be correlated to any specific behavior.

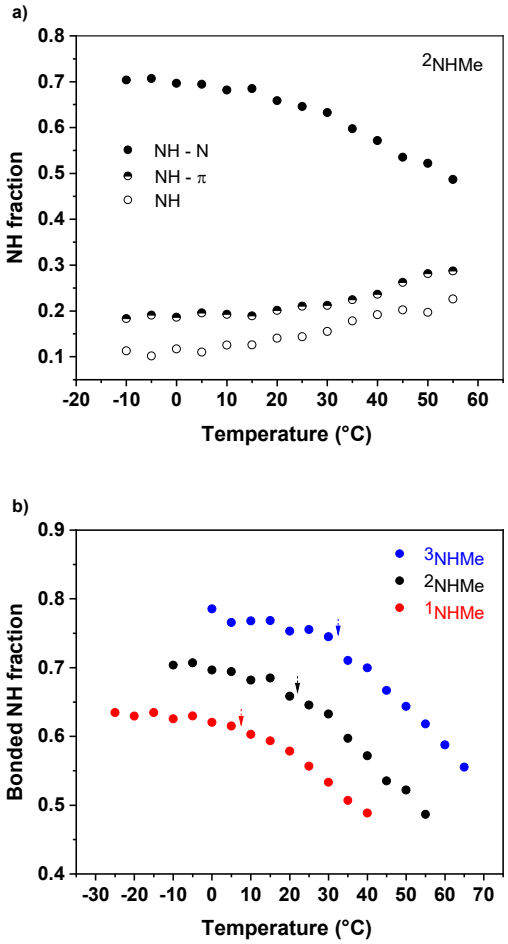

Figure 7. a) Fractions of NH groups engaged in hydrogen bonding (NH – N), NH – π interactions, and weak van der Waals interactions (NH) as a function of temperature for compound $\mathbf{2}_{NHMe}$. b) Hydrogen-bonded NH fraction as a function of temperature for compounds $\mathbf{1}_{NHMe}$-$\mathbf{3}_{NHMe}$.

Association Constants

Correlations were observed previously between the T_g of aminotriazine molecular glasses and the association constants (Ka) of their NH groups, which are indicative of hydrogen bond strength.[30, 50, 51] As the constants are measured by variable-concentration NMR spectroscopy in $CDCl_3$ solutions, we can assume that the impact of the weaker NH – π interactions is negligible. The Ka values of compounds $\mathbf{1}_{NHMe}$-$\mathbf{3}_{NHMe}$ (Table 3 and Figure S8) range from 0.2 to 0.4 M^{-1}. These small Ka values are substantially lower than that of their analogues with NH linkers, which typically ranged from 0.7 to 2.1 M^{-1}.[30, 50] This can be explained by the presence of only one NH group located on the headgroup. In our previous work, the headgroup NH

typically displayed a weaker Ka than the linker NH groups. More importantly, it can be observed that Ka increases with the presence of alkyl ancillary groups, with the Ka value for dicyclohexyl derivative $\mathbf{3}_{\mathbf{NHMe}}$ two times higher than that of diphenyl derivative $\mathbf{1}_{\mathbf{NHMe}}$ and mixed analogue $\mathbf{2}_{\mathbf{NHMe}}$ showing an intermediate value. These observations can be likely rationalized by the fact that alkylamino ancillary groups are stronger electron donors than arylamino groups due to the absence of resonance with the alkyl substituent. The electrons of the linker nitrogen atom are therefore more available for resonance with the triazine ring. Stronger resonance leads to higher electron density on the triazine nitrogen atoms, which become stronger H-bond acceptors. This resonance also led to the higher rotation energy barrier for the cyclohexyl ancillary groups in Figure 5. Interestingly, the mixed analogue $\mathbf{2}_{\mathbf{NHMe}}$ shows a Ka nearly 20 % higher than the average between symmetrical derivatives $\mathbf{1}_{\mathbf{NHMe}}$ and $\mathbf{3}_{\mathbf{NHMe}}$ which appears to be consistent with its T_g being somewhat closer to that of $\mathbf{3}_{\mathbf{NHMe}}$ than $\mathbf{1}_{\mathbf{NHMe}}$ (10 °C difference vs. 15 °C). The differences in Ka determined for compounds $\mathbf{1}_{\mathbf{NHMe}}$-$\mathbf{3}_{\mathbf{NHMe}}$ do not manifest themselves in the IR spectra of Figure 6. This may a consequence of the solution- vs bulk-state nature of the compounds in these two series of experiments. The steric hindrance of other molecules and the limited mobility in the bulk likely prevent the compounds from establishing optimal H-bonds.

Table 3. Association constants (Ka) for glasses $\mathbf{1}_{\mathbf{NHMe}}$, $\mathbf{2}_{\mathbf{NHMe}}$ and $\mathbf{3}_{\mathbf{NHMe}}$ determined by variable-concentration NMR spectroscopy in $CDCl_3$.

Compound	Ka (M^{-1})
1_{NHMe}	0.214 ± 0.003
2_{NHMe}	0.369 ± 0.001
3_{NHMe}	0.403 ± 0.002

Conclusions

The impact of alkyl, as opposed to aryl, ancillary cyclic substituents on triazine-based molecular glasses was probed with a library of twelve analogues containing either two phenyl or two cyclohexyl substituents, or one of each. All compounds showed excellent glass-forming ability, with no sign of crystallization upon slow cooling with a critical cooling rate systematically below 0.5 °C/min. The presence of cyclohexyl groups resulted in both higher glass transition temperatures (T_g) and lower glass kinetic stability. The higher T_g values are mainly attributable to higher rotational energy barriers for the cyclohexylamino groups, and to more extensive hydrogen bonding when NH groups are present thanks to the absence of competing NH – π interactions. The crystal structures of selected cyclohexyl or mixed analogues were determined and revealed that crystallization is driven by close packing rather than by the formation of specific intermolecular interactions. The cyclohexyl groups, which are bulkier than phenyl groups, seemingly decrease kinetic glass stability because their more efficient packing increases the thermodynamic drive toward crystallization.

Importantly, the results of this work demonstrate that the combination of aromatic substituents with a methylaminotriazine core provides an optimal molecular framework to combine excellent glass-forming ability and glass kinetic stability at room temperature in spite of a T_g as low as -19 °C. Considering the ease with which the aminotriazine core can be functionalized with various active moieties (such as azobenzenes, perylenediimides, etc.) that tend to increase the T_g of the resulting molecular glass, this work paves the way to the synthesis and exploitation of a broad range of functional amorphous molecular materials with sub-ambient glass transition temperature.

Experimental

General

2-Methylamino-4,6-dichloro-1,3,5-triazine,[26] 2-methoxy-4,6-dichloro-1,3,5-triazine,[33] 2-dimethylamino-4,6-dichloro-1,3,5-triazine,[32] 2-ethyl-4,6-dichloro-1,3,5-triazine,[34] 2-(N-methylphenylamino)-4,6-dichloro-1,3,5-triazine[35] and 2-methoxy-4,6-bis(N-methylphenylamino)-1,3,5-triazine[28] were synthesized according to previously published procedures. All other reagents were purchased from commercial sources and used without further purification. NMR spectra were recorded on a 400 MHz Bruker AV400 spectrometer at 298 K unless otherwise indicated.

The glass transition temperature (T_g) and melting temperature (T_m) were recorded by DSC with a PerkinElmer DSC 8500 calorimeter calibrated with indium using a heating rate of 10 °C/min. Transition temperatures were reported as an average over two runs after an initial cycle of heating and ballistic cooling to erase thermal history. Experiments to determine the critical cooling rates (R_c) were conducted by cooling the melted compounds at different rates ranging from 100 °C/min to 0.5 °C/min. For compounds without a melting temperature, the cooling scans were measured with a starting temperature corresponding to 2 % of weight loss as determined by thermogravimetric analysis using a TGA 2950 thermogravimetric analyzer (TA Instruments) with a 10 °C/min ramp in nitrogen. No sign of crystallization was observed for any compound either during the cooling scan or during the subsequent heating scan, indicating that $R_c < 0.5$ °C/min.

Infrared spectra with 4 cm^{-1} resolution were recorded on a Tensor 27 FT-IR spectrometer (Bruker Optics) equipped with a liquid nitrogen-cooled HgCdTe detector and a MIRacle (Pike Technologies) silicon attenuated total reflection (ATR) accessory. Thin films were directly cast on the ATR crystal from a $CHCl_3$ solution. For variable-temperature infrared spectroscopy studies, spectra were recorded with a resolution of 4 cm^{-1} using a Vertex 70 FT-IR spectrometer (Bruker Optics) equipped with a DTGS detector. An FTIR600 heating/cooling stage (Linkam Scientific Instruments) with IR-transparent windows and a T95 LinkPad controller were used to ramp the temperature. Samples were spin-coated on ZnSe windows from

$CHCl_3$ solutions and heated to 33 °C above T_g for 3 min to erase thermal history. Single beam spectra were then recorded at each 5 °C by averaging 50 scans during a cooling ramp at a rate of 2 °C/min. Background spectra were separately recorded for each temperature. The fractions of NH groups involved in H-bonds, van der Waals interactions or NH – π interactions were determined using a principal components analysis and a self-modeling mixture analysis procedure in PLS_Toolbox (Eigenvector Research). The procedure was similar to that previously reported by Laventure et al.[28] but using three principal components rather than two.

Synthesis of 2-ethyl-4,6-bis(N-methylphenylamino)-1,3,5-triazine ($\mathbf{1_{Et}}$)

To a round-bottomed flask equipped with a magnetic stirrer and a water-jacketed condenser, 2-ethyl-4,6-dichloro-1,3,5-triazine (1.00 g, 5.62 mmol) and N-methylaniline (1.34 mL, 1.32 g, 12.4 mmol) were dissolved in THF (25 mL), then the mixture was refluxed 18 h. After cooling down to ambient temperature, the volatiles were concentrated under vacuum, then the residue was redissolved in CH_2Cl_2. The solution was washed successively with 1M aq. HCl, H_2O and 1M aq. NaOH. The organic layer was recovered, dried over Na_2SO_4, filtered, and the volatiles were removed under reduced pressure to yield 1.58 g compound $\mathbf{1_{Et}}$ in acceptable purity (4.94 mmol, 88 %). T_g -19 °C; FT-IR (ATR) 3062, 3036, 2972, 2937, 2876, 1601, 1586, 1548, 1496, 1477, 1443, 1385, 1326, 1286, 1269, 1225, 1188, 1106, 1075, 1028, 977, 933, 905, 822, 764, 695 cm^{-1}; ^1H NMR (400 MHz, $CDCl_3$) δ 7.31 (m, 8H), 7.17 (t, *J* = 6.6 Hz, 2H), 3.46 (s, 6H), 2.54 (q, *J* = 7.5 Hz, 2H), 1.20 (t, *J* = 7.5 Hz, 3H) ppm; ^{13}C NMR (100 MHz, $CDCl_3$) δ 179.1, 165.2, 144.5, 128.3, 126.3, 125.2, 37.4, 32.1, 11.5 ppm; HRMS (ESI, MH^+) calcd. for $C_{19}H_{22}N_5$ *m/z*: 320.1870, found: 320.1864.

Compounds $\mathbf{1_{NHMe}}$ and $\mathbf{1_{NMe2}}$ were synthesized following the same procedure as compound $\mathbf{1_{Et}}$ (see ESI for details). from 2-methylamino-4,6-dichloro-1,3,5-triazine and 2-dimethylamino-4,6-dichloro-1,3,5-triazine, respectively (see ESI for details).

Synthesis of 2-(N-methylcyclohexylamino)-4-(N-methylphenylamino)-6-chloro-1,3,5-triazine (4)

2-(N-methylphenylamino)-4,6-dichloro-1,3,5-triazine (22.8 g, 89.4 mmol) was dissolved in acetone (100 mL) in a round-bottomed flask equipped with a magnetic stirrer. K_2CO_3 (12.4 g, 89.4 mmol) was added, then a solution of N-methylcyclohexylamine (11.7 mL, 10.1 g, 89.4 mmol) in acetone (50 mL) was added dropwise at ambient temperature. Once the addition complete, the mixture was stirred 12 h at ambient temperature, at which point the mixture was poured into H_2O. The precipitate was collected by filtration and washed with H_2O. The crude product was recrystallized from hot hexanes to yield 19.8 g compound **4** (59.7 mmol, 68 %). T_m 133 °C; FT-IR (ATR) 2928, 2852, 1600, 1560, 1487, 1445, 1395, 1315, 1245, 1160, 1100, 1025, 968, 799, 692 cm^{-1}; ^1H NMR (400 MHz, DMSO-d_6, 363 K) δ 7.41 (t, *J* = 7.0 Hz, 2H), 7.33 (d, *J* = 7.8 Hz, 2H), 7.26 (t, *J* = 7.3 Hz, 1H), 4.16 (br d, 1H), 3.43 (s, 3H), 2.90 (s, 3H), 1.78 (m, 2H), 1.61 (m, 3H), 1.50 (m, 2H), 1.11 (m, 1H) ppm; ^{13}C NMR (100 MHz, $CDCl_3$) δ 169.1, 164.9, 164.1, 143.9, 128.5, 126.4, 125.9, 54.7, 53.6, 37.9, 37.7, 29.9, 29.5, 28.5, 28.3, 25.7, 25.5 ppm; HRMS (ESI, MH^+) calcd. for $C_{17}H_{23}ClN_5$ *m/z*: 332.1637, found: 332.1632.

Synthesis of 2-methoxy-4-(N-methylcyclohexylamino)-6-(N-methylphenylamino)-1,3,5-triazine ($\mathbf{2_{OMe}}$)

2-(N-methylcyclohexylamino)-4-(N-methylphenylamino)-6-chloro-1,3,5-triazine **4** (2.00 g, 6.04 mmol) and sodium methoxide (25 wt% in MeOH, 1.96 mL, 9.06 mmol) were dissolved in MeOH (50 mL) in a round-bottomed flask equipped with a magnetic stirrer and a water-jacketed condenser. The mixture was refluxed 18 h, then, after cooling down to ambient temperature, the volatiles were concentrated under reduced pressure. The residue was redissolved in CH_2Cl_2, washed with H_2O, dried over Na_2SO_4, filtered, and thoroughly dried under vacuum to give 1.21 g of compound $\mathbf{2_{OMe}}$ (3.68 mmol, 61 %). T_g -5 °C; FT-IR (ATR) 3061, 3037, 3008, 2927, 2854, 1602, 1565, 1523, 1482, 1458, 1446, 1393, 1357, 1331, 1298, 1255, 1237, 1205, 1186, 1164, 1134, 1087, 1035, 1003, 962, 909, 894, 878, 811, 785, 765, 695 cm^{-1}; ^1H NMR (400 MHz, DMSO-d_6, 363 K) δ 7.34 (m, 4H), 7.21 (t, *J* = x Hz, 1H), 4.31 (br s, 1H), 3.76 (s, 3H), 3.44 (s, 3H), 3.01 (s, 3H), 1.77 (m, 2H), 1.61 (m, 3H), 1.48 (m, 2H), 1.23 (m, 2H), 1.11 (m, 1H) ppm; ^{13}C NMR (100 MHz, $CDCl_3$) δ 170.9, 166.2, 165.7, 144.7, 128.2, 126.4, 125.2, 54.2, 53.5, 37.3, 29.8, 28.2, 25.8, 25.6 ppm; HRMS (ESI, MH^+) calcd. for $C_{18}H_{26}N_5O$ *m/z*: 328.2132, found: 328.2126.

Synthesis of 2-methylamino-4-(N-methylcyclohexylamino)-6-(N-methylphenylamino)-1,3,5-triazine ($\mathbf{2_{NHMe}}$)

To a round-bottomed flask equipped with a magnetic stirrer and a water-jacketed condenser, 2-(N-methylcyclohexylamino)-4-(N-methylphenylamino)-6-chloro-1,3,5-triazine **4** (2.00 g, 6.04 mmol) and aqueous methylamine (40 wt%, 5 mL) were dissolved in THF (50 mL), then the mixture was refluxed 18 h. After cooling down to ambient temperature, the volatiles were concentrated under vacuum, then the residue was redissolved in CH_2Cl_2. The solution was washed successively with 1M aq. HCl, H_2O and 1M aq. NaOH. The organic layer was recovered, dried over Na_2SO_4, filtered, and the volatiles were removed under vacuum to yield, after thorough drying, 1.83 g compound $\mathbf{2_{NMe}}$ (5.60 mmol, 93 %). T_g 22 °C, T_m 79 °C; FT-IR (ATR) 3460, 3435, 3282, 3165, 3061, 3031, 2927, 2853, 1601, 1557, 1529, 1491, 1445, 1380, 1329, 1255, 1216, 1166, 1143, 1100, 1036, 1003, 894, 881, 809, 785, 758, 695, 666 cm^{-1}; ^1H NMR (400 MHz, $CDCl_3$) δ 7.34 (m, 4H), 7.15 (t, *J* = 6.9 Hz, 1H), 4.73 (br s, 1H), 4.35 (br s, 1H), 3.49 (s, 3H), 2.92 (s, 3H), 2.90 (s, 3H), 1.78 (m, 2H), 1.66 (m, 3H), 1.39 (m, 4H), 1.10 (m, 1H) ppm; ^{13}C NMR (100 MHz, $CDCl_3$) δ 166.7, 165.5, 165.0, 128.1, 126.5, 124.7, 53.4, 37.1, 30.0, 27.9, 27.4, 26.0, 25.8 ppm; HRMS (ESI, MH^+) calcd. for $C_{18}H_{27}N_6$ *m/z*: 341.2448, found: 341.2442.

Compound $\mathbf{2_{NMe2}}$ was synthesized following the same procedure as compound $\mathbf{2_{NHMe}}$ with aqueous dimethylamine (40 wt%) (see ESI for details).

Synthesis of 2-ethyl-4-(N-methylcyclohexylamino)-6-chloro-1,3,5-triazine (5)

2-Ethyl-4,6-dichloro-1,3,5-triazine (1.00 g, 5.62 mmol) was dissolved in acetone (20 mL) in a round-bottomed flask equipped with a magnetic stirrer. K_2CO_3 (0.780 g, 5.62 mmol) was added, then a solution of N-methylcyclohexylamine (0.742 mL, 0.636 g, 5.62 mmol) in acetone (10 mL) was added dropwise at ambient temperature. Once the addition was complete, the mixture was stirred 12 h at ambient temperature, then the mixture was poured into H_2O and stirred 30 min. The resulting precipitate was collected by filtration and washed briefly with hexanes to yield, after drying, 0.702 g compound **5** (2.76 mmol, 49 %). T_m x °C; FT-IR (ATR) 2930, 2852, 1608, 1565, 1487, 1412, 1322, 1282, 1252, 1160, 1028, 982, 879, 813 cm^{-1}; ^1H NMR (400 MHz, DMSO-d_6, 363 K) δ 4.44 (br d, 1H), 3.03 (s, 3H), 2.61 (q, *J* = 7.5 Hz, 2H), 1.82 (m, 2H), 1.65 (m, 3H), 1.57 (m, 2H), 1.36 (m, 2H), 1.21 (t, *J* = 7.4 Hz, 3H), 1.15 (m, 1H) ppm; ^{13}C NMR (100 MHz, $CDCl_3$) δ 180.3, 169.7, 164.5, 54.7, 54.1, 31.7, 29.6, 28.7, 25.4, 11.3 ppm; HRMS (ESI, MH^+) calcd. for $C_{12}H_{20}ClN_4$ *m/z*: 255.1371, found: 255.1368.

Synthesis of 2-ethyl-4-(N-methylcyclohexylamino)-6-(N-methylphenylamino)-1,3,5-triazine (2_{Et})

To a round-bottomed flask equipped with a magnetic stirrer and a water-jacketed condenser were added 2-ethyl-4-(N-methylcyclohexylamino)-6-chloro-1,3,5-triazine **5** (0.602 g, 2.36 mmol) and N-methylaniline (0.282 mL, 0.279 g, 2.60 mmol) in THF (20 mL), and the mixture was refluxed 18 h. After allowing the mixture to cool down to ambient temperature, the volatiles were concentrated under vacuum, then hexanes and 1M aq. HCl were added. The layers were separated, then the organic layer was washed with H_2O and 1M aq. NaOH, dried over Na_2SO_4, filtered, and the solvents were removed under reduced pressure to yield, after thorough drying, 0.667 g of compound $\mathbf{2_{Et}}$ (2.05 mmol, 87 %). T_g -18 °C; FT-IR (ATR) 3062, 3033, 2928, 2855, 1601, 1551, 1522, 1494, 1446, 1391, 1349, 1331, 1289, 1253, 1228, 1174, 1129, 1102, 1074, 1037, 975, 944, 894, 822, 764, 695 cm^{-1}; ^1H NMR (400 MHz, DMSO-d_6, 363 K) δ 7.35 (m, 4H), 7.20 (t, *J* = 6.3 Hz, 1H), 4.35 (br s, 1H), 3.45 (s, 3H), 2.91 (s, 3H), 2.44 (q, *J* = 7.4 Hz, 2H), 1.77 (m, 2H), 1.58 (m, 3H), 1.48 (m, 2H), 1.22 (m, 2H), 1.16 (t, *J* = 7.3 Hz, 3H), 1.11 (m, 1H) ppm; ^{13}C NMR (100 MHz, $CDCl_3$) δ 178.8, 165.1, 164.5, 144.9, 128.2, 126.4, 125.0, 53.8, 37.2, 32.2, 29.7, 28.0, 25.9, 11.6 ppm; HRMS (ESI, MH^+) calcd. for $C_{19}H_{28}N_5$ *m/z*: 326.2339, found: 326.2332.

Synthesis of 2-ethyl-4,6-bis(N-methylcyclohexylamino)-1,3,5-triazine (3_{Et})

To a round-bottomed flask equipped with a magnetic stirrer and a water-jacketed condenser, 2-ethyl-4,6-dichloro-1,3,5-triazine (1.00 g, 5.62 mmol) and N-methylcyclohexylamine (2.20 mL, 1.91 g, 16.9 mmol) were dissolved in THF (25 mL). K_2CO_3 (3.11 g, 22.5 mmol) was added, then the mixture was refluxed 18 h. After cooling down to ambient temperature, the volatiles were concentrated under vacuum, then the residue was redissolved in CH_2Cl_2. The solution was washed successively with 1M aq. HCl, H_2O and 1M aq. NaOH. The organic layer was recovered, dried over Na_2SO_4, filtered, and the volatiles were removed under reduced pressure to yield 1.61 g compound $\mathbf{3_{Et}}$ in acceptable purity (4.84 mmol, 86 %). T_g -8 °C, T_m 65 °C; FT-IR (ATR) 2926, 2853, 2796, 1550, 1519, 1486, 1449, 1399, 1378, 1348, 1328, 1259, 1251, 1219, 1191, 1170, 1121, 1075, 1036, 976, 894, 869, 837, 821, 802, 786, 744, 651 cm^{-1}; ^1H NMR (400 MHz, $CDCl_3$) δ 4.52 (br d, 2H), 3.00 (s, 6H), 2.53 (q, *J* = 6.9 Hz, 2H), 1.82 (m, 4H), 1.70 (m, 6H), 1.44 (m, 8H), 1.24 (t, *J* = 7.5 Hz, 3H), 1.13 (m, 2H) ppm; ^{13}C NMR (100 MHz, $CDCl_3$) δ 178.0, 164.8, 53.3, 32.2, 30.0, 28.0, 26.1, 25.8, 11.6 ppm; HRMS (ESI, MH^+) calcd. for $C_{19}H_{34}N_5$ *m/z*: 332.2809, found: 332.2803.
Compounds $\mathbf{3_{OMe}}$, $\mathbf{3_{NHMe}}$ and $\mathbf{3_{NMe2}}$ were synthesized following the same procedure as compound $\mathbf{3_{Et}}$ from 2-methoxy-4,6-dichloro-1,3,5-triazine, 2-methylamino-4,6-dichloro-1,3,5-triazine and 2-dimethylamino-4,6-dichloro-1,3,5-triazine, respectively (see ESI for details).

Crystal Structure Determination

Data were collected on a Bruker Venture Metaljet diffractometer using GaK_α radiation (λ = 1.34139 Å) During all experiments, samples were cooled using an Oxford Cryostream liquid-N_2 device at 150 K. Cell lattice parameters were determined using reflections taken from three sets of 104 frames (GaK_α instrument) or 180 frames (CuK_α instrument) measured and harvested within the *APEX3* suite of programs.[52] Integration of frames was performed using *SAINT*,[52] and a semiempirical absorption correction was applied with *SADABS*.[53] The structures were solved using a dual-space and intrinsic phasing approach with *SHELXT*,[54] and the refinement was carried out using *SHELXL*-2018/3[38] within the *OLEX2* suite of software.[55] The specimen used for compound $\mathbf{3_{NMe2}}$ turned out to be a two-components twin, the integration was performed using the two components to produce an HKLF5-type reflection file used for the refinement.

Variable-Concentration NMR Spectroscopy

For each compound, a 0.5 M stock solution was prepared in $CDCl_3$. Serial dilutions were performed and a volume of equivalent concentration of CH_2Cl_2 was added to each solution to calibrate the signal of NH groups in the NMR spectra. The spectra were then recorded at 298 K using a Bruker Avance 400 spectrometer. The 0.8 M solution was prepared by combining the compounds recuperated from the diluted solutions after recording their spectra, followed by complete drying and resolubilization in the proper volume of solvent. The association constant was determined using the chemical shift of the NH proton by fitting the data to the following equation:

$$P = (P_d - P_m)(1 + \frac{1 - \sqrt{8K_aC + 1}}{4K_aC}) + P_m$$

where *P* is the measured chemical shift, P_d is the theoretical shift of the dimer, P_m is the theoretical shift of the monomer, *C* is the concentration, and K_a is the equilibrium constant for dimerization.[51]

DFT Calculations

The geometries of compounds $\mathbf{1_{HG}}$ and $\mathbf{3_{HG}}$ with the bottom-bottom and top-bottom conformations of the ancillary groups were first optimized using Gaussian 16 with the B3LYP functional and the 6-311+G(d,p) basis set. Vibrational spectra were calculated to ensure the absence of imaginary frequencies. To determine the activation energy for rotation of the ancillary groups, scans of the dihedral angle of the bond between the linker N atom and the C3 or C5 atom of the triazine were conducted every 5° at the B3LYP/6-31G(d,p) level. At each step, the geometry of the rest of the molecule was optimized in order to reach a local minimum in energy. An analogous procedure was used to determine the activation energy for rotation of the headgroups, using the compounds in the bottom-bottom conformation. Computations were made on the supercomputer Graham managed by Compute Canada.

Conflicts of interest

There are no conflicts to declare.

Accession Codes

CCDC 19932284 – 19932287 contain the supplementary crystallographic data for this paper. These data can be obtained free of charge via www.ccdc.cam.ac.uk/data_request/cif, or by emailing data_request@ccdc.cam.ac.uk, or by contacting The Cambridge Crystallographic Data Centre, 12 Union Road, Cambridge CB2 1EZ, UK; fax: +44 1223 336033.

Acknowledgements

This research was funded by the Natural Sciences and Engineering Research Council of Canada (NSERC #RGPIN-2015-04014). We thank Compute Canada for access to the supercomputer Graham. The X-ray instrument used for the crystal structure determination was purchased through a grant from the Canada Foundation for Innovation.

Notes and references

1 M. D. Ediger, C. A. Angell and S. R. Nagel. *J. Phys. Chem.,* 1996**, 100**, 13200.
2 L. Berthier and M. D. Ediger. *Physics Today,* 2016**, 69**, 40.
3 K. A. Graeser, J. E. Patterson, J. A. Zeitler, K. C. Gordon and T. Rades. *Eur. J. Pharm. Sci.,* 2009**, 37**, 492.
4 D. Zhou, G. G. Zhang, D. Law, D. J. Grant and E. A. Schmitt. *J. Pharm. Sci.,* 2002**, 91**, 1863.
5 C. Bhugra and M. J. Pikal. *J. Pharm. Sci.,* 2008**, 97**, 1329.
6 J. F. Willart and M. Descamps. *Mol. Pharm.,* 2008**, 5**, 905.
7 T. Einfal, O. Planinsek and K. Hrovat. *Acta Pharm.,* 2013**, 63**, 305.
8 L. Yu. *Adv. Drug Deliv. Rev.,* 2001**, 48**, 27.
9 K. Iwata. *Polymer,* 2002**, 43**, 6609.
10 M. Habgood, R. W. Lancaster, M. Gateshki and A. M. Kenwright. *Cryst. Growth Des.,* 2013**, 13**, 1771.
11 Y. Shirota. *J. Mater. Chem.,* 2005**, 15**, 75.
12 P. Strohriegl and J. V. Grazulevicius. *Adv. Mater.,* 2002**, 14**, 1439.
13 S. F. Swallen, K. L. Kearns, M. K. Mapes, Y. S. Kim, R. J. McMahon, M. D. Ediger, T. Wu, L. Yu and S. Satija. *Science,* 2007**, 315**, 353.
14 S. Tominaka, K. Kawakami, M. Fukushima and A. Miyazaki. *Mol. Pharm.,* 2017**, 14**, 264.
15 Z. Wojnarowska, K. Grzybowska, L. Hawelek, M. Dulski, R. Wrzalik, I. Gruszka, M. Paluch, K. Pienkowska, W. Sawicki, P. Bujak, K. J. Paluch, L. Tajber and J. Markowski. *Mol. Pharm.,* 2013**, 10**, 3612.
16 A. De Silva, N. M. Felix and C. K. Ober. *Adv. Mater.,* 2008**, 20**, 3355.
17 R. Walker, H. Audorff, L. Kador and H.-W. Schmidt. *Adv. Funct. Mater.,* 2009**, 19**, 2630.
18 F. Krohn, C. Neuber, E. A. Rossler and H. W. Schmidt. *J. Phys. Chem. B,* 2019**, 123**, 10286.
19 A. Minecka, E. Kaminska, M. Tarnacka, I. Grudzka-Flak, M. Bartoszek, K. Wolnica, M. Dulski, K. Kaminski and M. Paluch. *Mol. Pharm.,* 2018**, 15**, 4764.
20 A. Kalra, M. Zhang, S. Parkin and T. Li. *Z. Kristallogr. Cryst. Mater.,* 2018**, 233**, 9.
21 N. Van den Brande, A. Gujral, C. Huang, K. Bagchi, H. Hofstetter, L. Yu and M. D. Ediger. *Cryst. Growth Des.,* 2018**, 18**, 5800.
22 K. Kawakami, T. Harada, K. Miura, Y. Yoshihashi, E. Yonemochi, K. Terada and H. Moriyama. *Mol. Pharm.,* 2014**, 11**, 1835.
23 A. Kalra, P. Luner, L. S. Taylor, S. R. Byrn and T. Li. *J. Pharm. Sci.,* 2018**, 107**, 192.
24 O. Lebel, T. Maris, M. E. Perron, E. Demers and J. D. Wuest. *J. Am. Chem. Soc.,* 2006**, 128**, 10372.
25 J. D. Wuest and O. Lebel. *Tetrahedron,* 2009**, 65**, 7393.
26 R. N. Eren, A. Plante, A. Meunier, A. Laventure, Y. Huang, J. G. Briard, K. J. Creber, C. Pellerin, A. Soldera and O. Lebel. *Tetrahedron,* 2012**, 68**, 10130.
27 A. Laventure, A. Soldera, C. Pellerin and O. Lebel. *New J. Chem.,* 2013**, 37**, 3881.
28 A. Laventure, G. De Grandpre, A. Soldera, O. Lebel and C. Pellerin. *Phys. Chem. Chem. Phys.,* 2016**, 18**, 1681.
29 R. Y. Wang, C. Pellerin and O. Lebel. *J. Mater. Chem.,* 2009**, 19**, 2747.
30 A. Plante, D. Mauran, S. P. Carvalho, J. Y. Page, C. Pellerin and O. Lebel. *J. Phys. Chem. B,* 2009**, 113**, 14884.
31 A. Plante, S. Palato, O. Lebel and A. Soldera. *J. Mater. Chem. C,* 2013**, 1**, 1037.
32 T. Matsuno, M. Kato, Y. Tsuchida, M. Takahashi, S. Yaguchi and S. Terada. *Chem. Pharm. Bull.,* 1997**, 45**, 291.
33 T. Tanaka, M. Noguchi, K. Watanabe, T. Misawa, M. Ishihara, A. Kobayashi and S. Shoda. *Org. Biomol. Chem.,* 2010**, 8**, 5126.
34 J. P. Whitten, Y. F. Xie, P. E. Erickson, T. R. Webb, E. B. De Souza, D. E. Grigoriadis and J. R. McCarthy. *J. Med. Chem.,* 1996**, 39**, 4354.
35 S. Fujii, T. Kobayashi, A. Nakatsu, H. Miyazawa and H. Kagechika. *Chem. Pharm. Bull.,* 2014**, 62**, 700.
36 K. Kunal, C. G. Robertson, S. Pawlus, S. F. Hahn and A. P. Sokolov. *Macromolecules,* 2008**, 41**, 7232.
37 A. Laventure, T. Maris, C. Pellerin and O. Lebel. *Cryst. Growth Des.,* 2017**, 17**, 2365.
38 G. M. Sheldrick. *Acta Crystallogr. C,* 2015**, C71**, 3.
39 A. I. Kitaigorodskii, *Molecular crystals and molecules*. Academic Press: New York, 1973.

40 A. L. Spek. *J. Appl. Crystallogr.,* 2003**, 36**, 7.
41 P. van der Sluis and A. L. Spek. *Acta Crystallogr. A,* 1990**, 46**, 194.
42 J. J. McKinnon, A. S. Mitchell and M. A. Spackman. *Chem.: Eur. J.,* 1998**, 4**, 2136.
43 M. A. Spackman and J. J. McKinnon. *CrystEngComm,* 2002**, 4**, 378.
44 J. J. McKinnon, F. P. A. Fabbiani and M. A. Spackman. *Cryst. Growth Des.,* 2007**, 7**, 755.
45 M. J. Turner, J. J. McKinnon, S. K. Wolff, D. J. Grimwood, P. R. Spackman, D. Jayatilaka and M. A. Spackman, *CrystalExplorer17* 2017; University of Western Australia.
46 A. P. Hyengoyan, S. S. Mamyan, T. A. Gomktsyan, E. N. Hambardzumyan, A. S. Vorskanyan, K. A. Eliazyan, V. A. Pivazyan and V. V. Dovlatyan. *Chem. Heterocycl. Compd.,* 2005**, 41**, 1059.
47 M. A. Trachsel, P. Ottiger, H. M. Frey, C. Pfaffen, A. Bihlmeier, W. Klopper and S. Leutwyler. *J. Phys. Chem. B,* 2015**, 119**, 7778.
48 C. T. Lin, S. W. Kuo, J. C. Lo and F. C. Chang. *J. Phys. Chem. B,* 2010**, 114**, 1603.
49 A. Choperena and P. Painter. *Macromolecules,* 2009**, 42**, 6159.
50 A. Laventure, D. Lauzon, C. Pellerin and O. Lebel. *CrystEngComm,* 2019**, 21**, 1734.
51 K. M. Psutka and K. E. Maly. *RSC Adv.,* 2016**, 6**, 78784.
52 Bruker, *APEX3 and SAINT*, 2017; Madison, WI.
53 L. Krause, R. Herbst-Irmer, G. M. Sheldrick and D. Stalke. *J. Appl. Crystallogr.,* 2015**, 48**, 3.
54 G. M. Sheldrick. *Acta Crystallogr. A,* 2015**, A71**, 3.
55 O. V. Dolomanov, L. J. Bourhis, R. J. Gildea, J. A. K. Howard and H. Puschmann. *J. Appl. Crystallogr.,* 2009**, 42**, 339.

